Segmental Track Analysis in Dynamic Wireless Power Transfer

Shi-Chun Yang [1], Hong He [1], Xiao-Yu Yan [1],*, Yu-Hang Chen [1], Yang Hua [1], Yao-Guang Cao [1], Jun Li [2], Hong-Hai Li [3],* and Sheng Yin [3]

[1] School of Transportation Science and Engineering, Beihang University, Beijing 100191, China; yangshichun@buaa.edu.cn (S.-C.Y.); he13131073@163.com (H.H.); chenyuhang1@buaa.edu.cn (Y.-H.C.); 13910710182@163.com (Y.H.); caoyg2006@126.com (Y.-G.C.)

[2] School of Vehicle and Mobility, Tsinghua University, Beijing 100084, China; lijun_beihang@163.com

[3] Research Institute of Highway Ministry of Transport, Beijing 100088, China; yinsheng@itsc.cn

* Correspondence: yanxiaoyu@buaa.edu.cn (X.-Y.Y.); llh@itsc.cn (H.-H.L.)

Abstract: Electric vehicles have gained more and more attention because of the serious oil crisis and environmental problems. However, the disadvantages of the electric vehicle, such as short driving range, high battery cost, and inconvenient charging, are hindering its market development and expansion. The realization of on-road wireless power transfer technology can effectively solve the problems of short driving range, prevent the battery from being completely discharged to prolong its service life, and reduce requirement of on-board battery. In this paper, the charging mode and the compensation topology of wireless power transfer technology are discussed and then the equivalent circuit model of segmental wireless power transfer system is built. We carried out some magnetic field simulation to analyze how the track shape and length influence coupling coefficient, which is later verified by experiments.

1. Introduction

Wireless power transfer technology, which is safe, robust, reliable, and convenient compared with conventional conductive charging method, can help to improve consumers' charging experience and promote expansion of the electric vehicle (EV) market greatly. Therefore it has gained more and more attention and applications in the EV industry. Moreover, with the development of electronic components, the technology that charges the EV while driving, namely dynamic wireless power transfer, has a quite promising future since it makes the charging operation flexible and reduces requirements of on-board battery effectively.

Inductive power transfer technology is widely adopted in dynamic wireless power transfer system because it has a better compromise between the working frequency, transfer distance, power level, and system efficiency than other technologies, taking electric field resonance for example of which working frequency reaches up to 2 MHz [1]. The inductive dynamic wireless power transfer track can be sorted into lumped track and stretched track. For the former, a number of transmit coils are arranged in sequence under the road surface to charging the mobile receivers. Double-D-Quadrature (DDQ) coils [2] proposed by Auckland University are preferred for the pickup side to eliminate the power null phenomenon [3] while a comparative analysis of other coil shapes for the primary side has also been carried out [4,5]. In order to obtain a stable output power under the condition of discontinuous primary power transfer, additional measures are essential. To this end, several control strategies are put forward in [6,7] and an equivalent model to analyze the switch-on process of dynamic wireless power transfer

system is proposed in [8]. Another method is to arrange transmitter coils closely to reduce the power pulsation between two adjacent coils, which will, however, result in self-coupling on the primary side. Compensation topologies could also be a solution, LCC compensation topology for example [6,9], are introduced in the primary circuit to solve this problem. Stretched track can be further divided into single-loop track and segmental track, both allow multi pickups being coupled simultaneously and have the merit of less electric convert and control devices and less cost for a given length charging road. However, the former suffers from the low coupling coefficient and serious electromagnetic field (EMF) problem due to large leakage flux. To address this issue, ferrite is of vital importance to enhance the coupling and in this aspect, it is notable that Korea Advanced Institute of Technology (KAIST) has started related researching work since the 1990s and has developed 6 generations of online electric vehicles (OLEV), of which the ferrite structure, power transfer distance, power transfer capability, and system efficiency are increasingly improved [10–14]. Furthermore, an optimization algorithm with the objective to minimize the investment cost by diminishing the utilized ferrite material is proposed by KAIST recently and it has proved the feasibility of none ferrite track theoretically [15]. Another problem of the single-loop track is reliability, because it utilizes an integrated circuit and control system, where a failure of one component will lead to unavailability of the entire charging system.

This paper focus on the segmental track analysis and a handful researches have been done before. Chongqing University established a nonlinear programming mathematical model, considering the layout of rails, the capacity of devices and the voltage level, with the objective to minimize the operation cost to plan segmental track length. The particle swarm optimization (PSO) algorithm is introduced to find the optimum solution [8] in their work. Besides, Hongkong Polytechnic University focused on the system efficiency to acquire an optimized track length based on the elaborated study of relationship among various key parameters such as vehicle speed, power utilization, track length, and system efficiency [16]. In this paper, the track length of primary track was studied mainly by taking system stability into account and the paper is organized as follows: The basic compensation topologies and system circuit model is analyzed in Section 2; In Section 3, circuit simulation was carried out to verify the correctness of theory analysis at first, and then the magnetic field simulation with FEA (finite element analysis) model and track analysis are elaborated; Experimental verification is presented in Section 4, while some conclusions are summarized in Section 5 at last.

2. Dynamic Charging System Circuit Model Analysis

2.1. Basic Compensation Topologies

The power transfer part of the charging system can be simplified to a loosely coupled transformer. Due to the relatively large air gap between transmit coil and receive coil, the magnetic flux leakage problem is serious, which reduces the voltage gain, power factor and transmission energy capability of the whole system. To address this matter, the widely utilized method is to subjoin compensate topology to resonate the circuits, increase the power factor and system efficiency [17]. Assuming power receivers are identical and decoupled with each other and transmitting track has same coupling strength with every receiver, the compensation topologies can be divided into four basic types based on the way the capacitors connected to the circuits (series or parallel with the coil) as shown in Figure 1, while the more complicated compensation topologies like LCC are not within the scope in this paper. They are SS (series–series) compensation topology, SP (series–parallel) compensation topology, PS (parallel–series) compensation topology, PP (parallel–parallel) compensation topology. In the simplified circuit model with compensation topology, U_1 stands for the inverted AC input power, L_P and L_s are the self-inductance of the transmitting and receiving coil respectively, R_P and R_s represent the cable resistance value of transmitting and receiving side respectively, C_p and C_s are the compensation capacitances of the transmitting and receiving side circuits respectively. M means the mutual inductance between the transmitting coil and the receiving coil, the load of the battery is roughly equivalent to a resistance R here.

(**a**) SS compensation topology

(**b**) PS compensation topology

(**c**) SP compensation topology

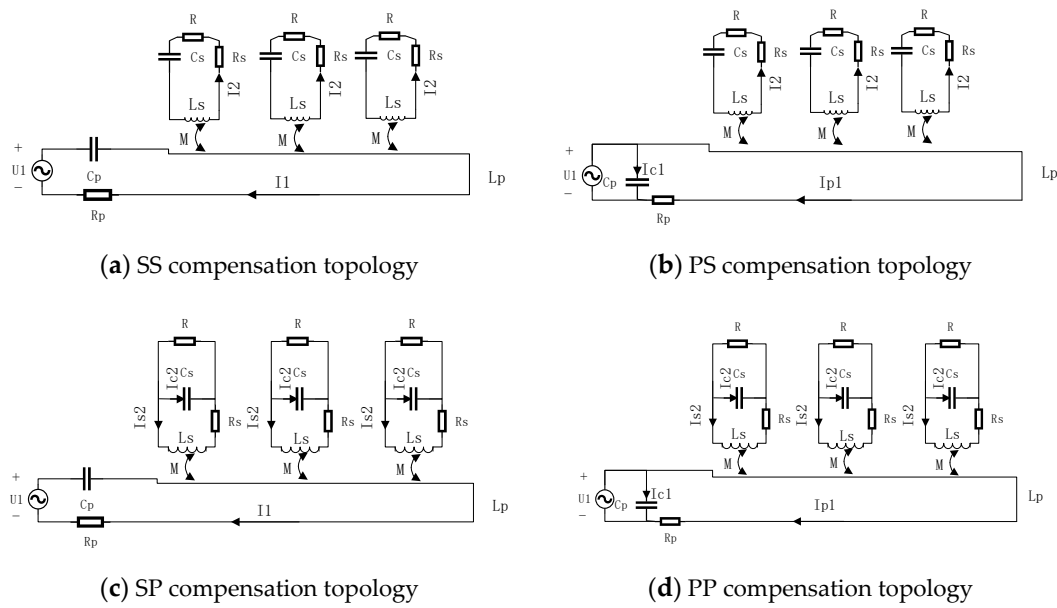(**d**) PP compensation topology

Figure 1. Four basic compensation topologies of inductive wireless power transfer system. PP—parallel–parallel; PS—parallel–series; SP—series–parallel; S—series–series.

The characteristics of different compensation topologies vary under different load and the coupling coefficient condition [18,19]. Therefore, the appropriate compensation topology needs to be chosen according to the specific application. For a preliminary analysis, the coil resistance R_P, R_s is ignored because they are relatively very small to the load resistance.

The impedance on single receiver is:

$$Z_s = \begin{cases} j\omega L_s + \frac{1}{j\omega C_s} + R \ (-S) \\ j\omega L_s + \frac{1}{j\omega C_s + \frac{1}{R}} \ (-P) \end{cases} \tag{1}$$

where the -S represents load side series compensated topologies and -P represents load side parallel compensated ones. The effect of the load side on the power supply side can be expressed in terms of the reflected impedance, which can be expressed as:

$$Z_r = \frac{\omega^2 M^2}{Z_s} \tag{2}$$

Bring Equation (1) into (2), the real part and the imaginary part of reflected resistance are obtained:

$$R_e Z_r = \begin{cases} \frac{\omega^4 C_s^2 M^2 R}{\left(\omega^2 C_s L_s - 1\right)^2 + \omega^2 C_s^2 R^2} \ (-S) \\ \frac{\omega^2 M^2 R}{R^2 \left(\omega^2 C_s L_s - 1\right)^2 + \omega^2 L_s^2} \ (-P) \end{cases} \tag{3}$$

$$I_m Z_r = \begin{cases} \frac{-\omega^3 C_s M^2 \left(\omega^2 C_s L_s - 1\right)}{\left(\omega^2 C_s L_s - 1\right)^2 + \omega^2 C_s^2 R^2} \ (-S) \\ \frac{-\omega^3 M^2 \left[C_s R^2 \left(\omega^2 C_s L_s - 1\right) + L_s \right]}{R^2 \left(\omega^2 C_s L_s - 1\right)^2 + \omega^2 L_s^2} \ (-P) \end{cases} \tag{4}$$

The power delivered to the load side by the power supply can be simply expressed as:

$$P = (R_e Z_r) I_P^2 \tag{5}$$

where I_p is the current flowing through the transmitting track. The resonant frequency of the secondary side is:

$$\omega_0 = \frac{1}{\sqrt{C_s L_s}} \tag{6}$$

When system working frequency is the resonant frequency of the secondary circuit, the impedance of the secondary side is:

$$R_e Z_{r0} = R_e Z_r(\omega = \omega_0) = \begin{cases} \frac{\omega_0^2 M^2}{R} \ (-S) \\ \frac{M^2 R}{L_s^2} \ (-P) \end{cases} \tag{7}$$

$$I_m Z_{r0} = \begin{cases} 0 \ (-S) \\ -\frac{\omega_0 M^2}{L_s} \ (-P) \end{cases} \tag{8}$$

The total system load impedance seen from the power supply end is:

$$Z_t = \begin{cases} \frac{1}{j\omega C_p} + j\omega L_p + N Z_r \ (S-) \\ \frac{1}{j\omega C_p + \frac{1}{j\omega L_p + N Z_r}} \ (P-) \end{cases} \tag{9}$$

N appeared in the equation means the number of receivers coupled with one single rail, S- represents the power supply side series-compensated topology and P- represents the parallel-compensated ones. The real part of the reflected impedance represents the active power part and the imaginary part is the reactive power of the system transmitting energy. In order to increase the active power delivered by the entire system, reactive power should be minimized, preferably to zero. This requires the system to work at the appropriate operating frequency, so that the impact of capacitance and inductance offset. To this end, the resonant frequency of primary circuit should be identical with that of the secondary circuit to further enhance the energy transmission capability of the system.

Therefore, the following relationship needs to be met:

$$I_m Z_t(\omega = \omega_0) = 0 \tag{10}$$

Power supply side compensation capacitor C_p can be obtained:

$$C_p = \begin{cases} \frac{1}{\omega_0^2 L_p} \ (SS) \\ \frac{L_p}{\left(N^2 \omega_0^2 M^2 / R\right)^2 + \omega_0^2 L_p^2} \ (PS) \\ \frac{1}{\omega_0^2 (L_p - N M^2 / L_s)} \ (SP) \\ \frac{L_p - N M^2 / L_s}{\left(N M^{2R} / L_s^2\right)^2 + \omega_0^2 (L_p - N M^2 / L_s)^2} \ (PP) \end{cases} \tag{11}$$

In the actual usage of the wireless power transfer system on electric vehicles, the equivalent resistance of the battery varies with the state of battery and the actual state of vehicle. Meanwhile, the change of the relative position of the primary coil and the secondary coil leads to mutual inductance non-constant. Analyze the calculated compensation capacitor value from (11) on the primary side, it can be told that primary compensation capacitance needs varying with load R, mutual inductance M and number of coupled receiver N all the time to keep the system resonant under PS, PP, SP compensation topologies, which is not feasible. Therefore, SS topology is chosen for further analysis because its primary compensation capacitance is independent on the load and mutual inductance, which suits dynamic charging system better.

2.2. Equivalent Circuit Model Analysis

Figure 2 shows the equivalent circuit model of multi receivers coupled wireless power transfer system where R_p and R_s are the internal resistance of the primary and secondary coils respectively, and R_0 is the equivalent resistance of the load. Assuming that the mutual inductance between a single receiver and the primary side is M, the impedance of a single secondary winding according to (1) is:
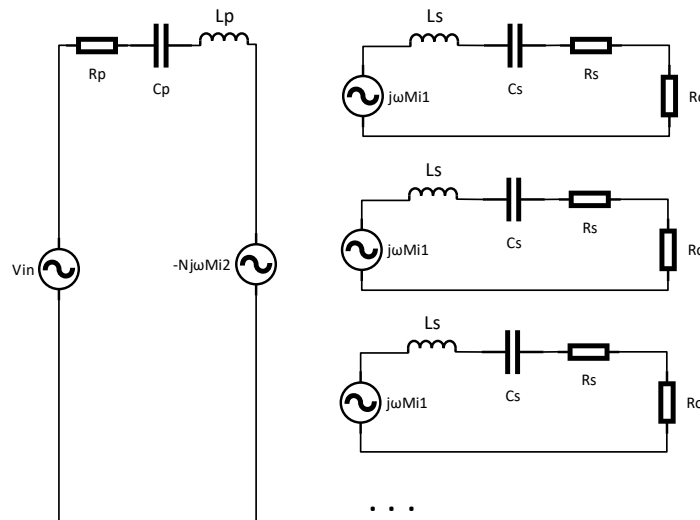

Figure 2. Equivalent circuit of wireless power transfer system.

$$Z_2 = \omega L_s + \frac{1}{j\omega C_s} + R \tag{12}$$

where R is the sum of the internal resistance of the secondary coil and the equivalent resistance of the load, $R = R_s + R_0$. According to Equations (3) and (4), the real and imaginary parts of the reactance of a single secondary winding on the primary side are:

$$Z_r = \begin{cases} \dfrac{\omega^4 C_s^2 M^2 R}{\left(\omega^2 C_s L_s - 1\right)^2 + \omega^2 C_s^2 R^2} & (\text{Re}) \\ j\dfrac{-\omega^3 C_s M^2 \left(\omega^2 C_s L_s - 1\right)}{\left(\omega^2 C_s L_s - 1\right)^2 + \omega^2 C_s^2 R^2} & (\text{Im}) \end{cases} \tag{13}$$

Assuming that a rail is coupled with N identical power receivers, according to (9), the real and imaginary parts of the primary impedance seen from the power supply are:

$$Z_t = \begin{cases} \dfrac{N\omega^4 C_s^2 M^2 R}{\left(\omega^2 C_s L_s - 1\right)^2 + \omega^2 C_s^2 R^2} + R_p & (\text{Re}) \\ j\left[\dfrac{-N\omega^3 C_s M^2 \left(\omega^2 C_s L_s - 1\right)}{\left(\omega^2 C_s L_s - 1\right)^2 + \omega^2 C_s^2 R^2} + \omega L_p - \dfrac{1}{\omega C_p}\right] & (\text{Im}) \end{cases} \tag{14}$$

The impedance angle of the primary impedance is:

$$\varphi = \arctan \frac{-N\omega^3 C_s M^2 \left(\omega^2 C_s L_s - 1\right) + \left[\left(\omega^2 C_s L_s - 1\right)^2 + \omega^2 C_s^2 R^2\right]\left(\omega L_p - \frac{1}{\omega C_p}\right)}{N\omega^4 C_s^2 M^2 R + \left[\left(\omega^2 C_s L_s - 1\right)^2 + \omega^2 C_s^2 R^2\right] R_p} \tag{15}$$

where λ is the ratio of the operating frequency and the resonant frequency, $\lambda = \frac{\omega}{\omega_0}$. When $\lambda = 1$, the frequency is called the natural resonant frequency. The coupling coefficient $k = \frac{M}{\sqrt{L_p L_s}}$, the secondary

quality factor $Q_s = \frac{\omega_0 L_s}{R}$, and $q = \frac{R_p}{\omega_0 L_p}$. Bringing the parameters above into Equation (15), it can be simplified:

$$\varphi = \arctan \frac{k^2 Q_s N(\lambda^2 - 1)[-\lambda^4 k^2 Q_s^2 N + Q_s^2(\lambda^2 - 1)^2 + \lambda^2]}{\lambda^5 k^2 Q_s N + [Q_s^2(\lambda^2 - 1)^2 + \lambda^2]\lambda q} \tag{16}$$

Output power of single receiver is:

$$P = \text{Re} \frac{(j\omega I_1)^2 R_0}{(j\omega L_s + \frac{1}{j\omega C_s} + R)R} = \frac{\lambda^4 M^2 I_1^2 R_0 \omega_0^2}{[(1 - \lambda^2)^2 Q_s^2 + \lambda^2]R^2} \tag{17}$$

From (16), we can see that the impedance angle of the primary side is related to four coefficients including the coupling coefficient k, the secondary quality factor Q_s, the operating frequency and the resonant frequency ratio λ, and the coefficient q. When the impedance angle is zero, the entire system is in resonance. When the parameters are chosen inappropriately during the design process, the point where the impedance angle is zero is not unique, which means the occurrence of frequency bifurcation phenomenon. Under this situation, the stability of the system decreases, the sensitivity of the parameters increases. To ensure that the inductive wireless power transfer system avoids frequency bifurcation, the Equation (16) has only one positive solution ($\lambda = 1$) to the equation about λ, that is, its discriminant (19) is less than zero.

$$-\lambda^4 k^2 Q_s^2 N + Q_s^2(\lambda^2 - 1)^2 + \lambda^2 = 0 \tag{18}$$

$$\Delta = 4k^2 Q_s^4 N - 4Q_s^2 + 1 < 0 \tag{19}$$

$$N < \frac{4Q_s^2 - 1}{4Q_s^4 k^2} \tag{20}$$

From the discussion above, it can be known that the characteristic Δ is a function of number of single-rail coupled receivers N when the system parameters are all set constant. Therefore, the maximum number N of receivers on a single rail design should satisfy the Equation (20).

3. Simulation Analysis and Track Length Plan Algorithm

3.1. Circuit Simulation and Analysis

In the Section 2, the conclusion that the number of receiving coils, a given track could bear, should satisfy the Equation (20) to avoid frequency bifurcation. To verify the correctness of the theory analysis, here in this section, circuit models of one transmitter with different number of receivers are built in Simulink of MATLAB (2015b, MathWorks, Natick, MA, USA) to test system performance. Assume that $Q_s = 6$ and $k = 0.1$, and according to Equation (20), the number of receivers, N, should be:

$$N < \frac{4Q_s^2 - 1}{4Q_s^4 k^2} = 2.75$$

Theoretically, there should be no more than two receiving coils. Based on that, circuit models with two receivers and three receivers are built as a contrast group to check what will happen when the number of receivers exceeds the limitation, and the latter is shown in Figure 3 which only has one more coil and one more receiver than that of two receivers.
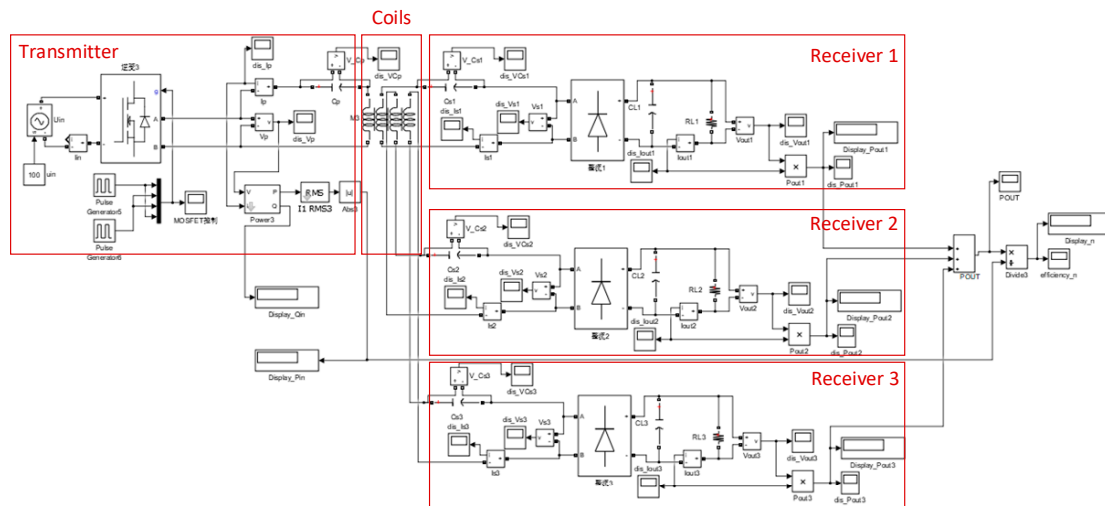
Figure 3. Circuit model of wireless charging system with three receivers in Simulink.

In this simulation, the same assumption as Section 2, that all the receivers are with same self-inductance, resistance, coupling coefficient and load, is put forward here. More detailed parameters of the simulation circuit are listed in Table 1 below.

**Table 1.** Parameters involved in circuit model.

Parameter	Value
Input voltage/P_{in}	100 V
Resonant frequency/f	100 kHz
Coupling coefficient between transmitter and receivers/k	0.1
Self-inductance of transmitting coil/L_p	120 µH
Primary compensation capacitance/C_p	21.1 nF
Self-inductance of receiving coils/L_{s1}, L_{s2}, L_{s3}	120 µH
Secondary compensation capacitance/C_{s1}, C_{s2}, C_{s3}	21.1 nF
Secondary quality factor/Q_s	6
Load resistance/R_{L1}, R_{L2}, R_{L3}	2 Ω

Based on the circuit models, the simulation is completed and the curves of output power and efficiency changing with time are shown in Figure 4.
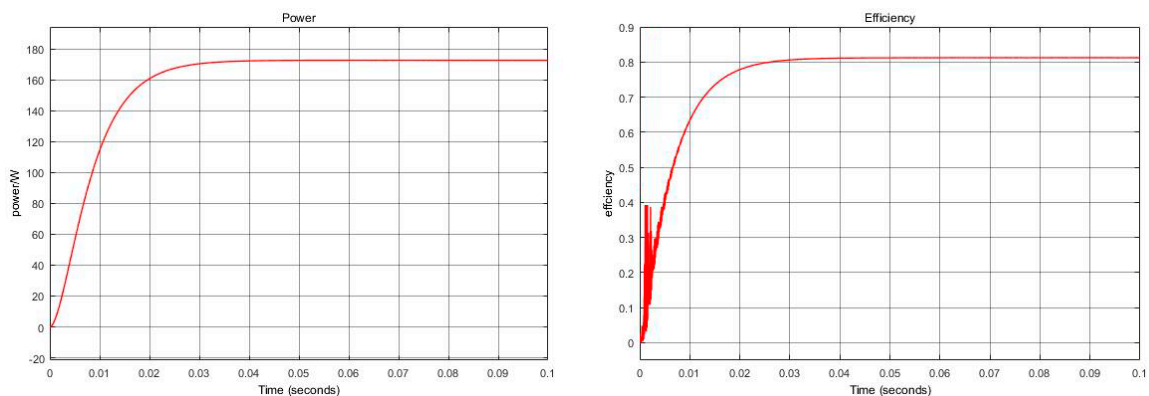
(**a**) Efficiency and added output power of system with two receivers

Figure 4. *Cont.*
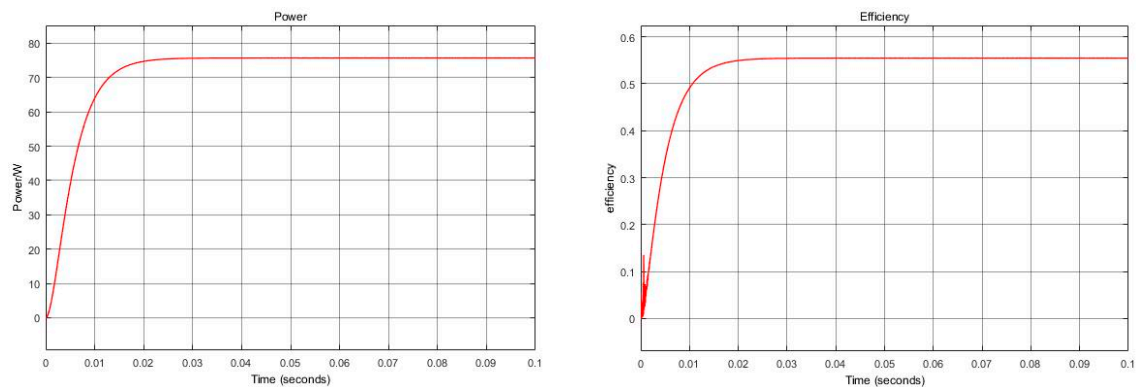
(**b**) Efficiency and added output power of system with three receivers

Figure 4. Output power and efficiency of the two systems.

Comparing the added output power curves of the two models, it can be easily found that there is an obvious drop in the power from 172 W to 76 W when the number of receivers increases from two to three. Similarly, a significant decrease of 25.8% in efficiency occurs when the number of receivers exceeds the limitation, with the system efficiency is 81.2% when two receivers and 55.4% when three receivers. The great decrease in both power and efficiency indicates the occurrence of frequency bifurcation when the number of receivers exceeds the limitation presented in Equation (20), which is consistent with the conclusion of theoretical analysis.

3.2. Magnetic Field Simulation and Analysis

Circular receiving coil is widely adopted on vehicles due to its slight superior performance in lateral misalignment and coupling effectiveness than other simple shape coils [20]. Therefore, for practical considerations, the receiving coil was set as a circular pad in the study. Also, the magnetic field simulation, the different shapes of the primary track, including the racetrack and rectangle, the most used shapes are first discussed. Then, the coupling coefficient between the same circular receiving coil and track with different length is analyzed in detail because it is closely related to output power and system efficiency. In this paper, the track length of 2d (two times of diameter of receiving coil) and 3d (three times of diameter of receiving coil) are chosen to be compared simply due to limited calculation resource and longer tracks will be further studied in the future work.

3.2.1. Track Length Analysis with Single Receiving Coil

As shown in Figure 5, the racetrack and rectangle tracks with a length 2d and 3d, assuming the diameter of the receiving coil is d, are studied respectively. Moreover, all the tracks are wrapped the same number of turns using the same wire in the same way. During the simulation, there are isometric points with which center of the receiving coil is going to be aligned. During the charging process, the motion speed will also influence the vehicle density and thus the number of receivers coupled with a given length track, which has been carefully analyzed in [18] and is not in the scope of this work. Therefore both the transmitting track and receiving coil are static at each simulation point and analyzed from point 1 to point 3 or 5. Taking 2d racetrack for example, there are actually three simulation models since there are three simulation points as shown in Figure 6. Simulation related parameters are listed in Table 2.
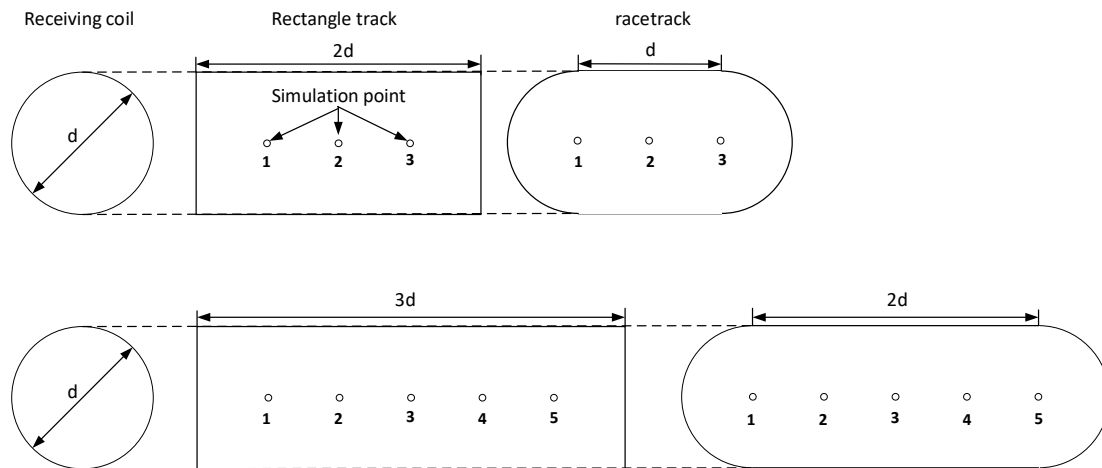
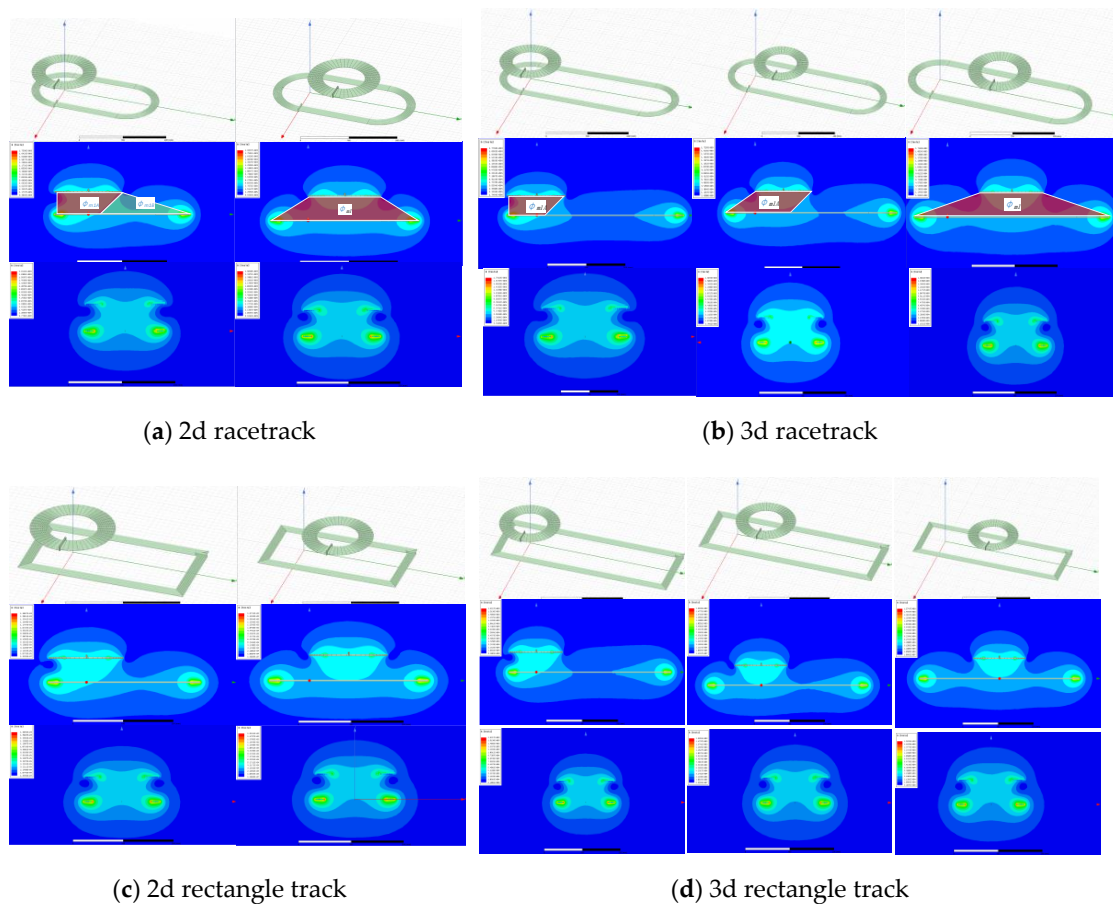**Figure 5.** Schematic diagram of shape and size of receiving coil and tracks.

(**a**) 2d racetrack

(**b**) 3d racetrack

(**c**) 2d rectangle track

(**d**) 3d rectangle track

Figure 6. Models and magnetic distribution of racetrack and rectangle with 2d and 3d length.

Table 2. Simulation related parameters.

Diameter d /mm	Receiving Coil Turns N	Track Turns N	Wire Diameter d_w/mm	Distance h/mm	Transmit Current I_1/A	Receive Current I_2/A
150	10	6	3	50	6	2

The simulation models built in MAXWELL (18.2, ANSYS, Pittsburgh, PA, USA) and magnetic field distributions on XZ plane and YZ plane of each model are obtained with part of them shown

in Figure 6 considering that they are symmetrical about the center. For better illustration the red quadrilateral marks are added to show the strong flux supported by the left/right side of the track, and the green quadrilaterals represent relatively weak flux. The coupling coefficient at different test points of each track are listed in Table 3.

Table 3. 3 Coupling coefficients at different points.

Points	1	2	3	4	5	Average
2dracetrack	0.1512	0.1653	0.1531			0.1565
2drectangle	0.1400	0.1456	0.1424			0.1427
3dracetrack	0.1225	0.1300	0.1275	0.1306	0.1240	0.1269
3drectangle	0.1178	0.1197	0.1174	0.1196	0.1184	0.1186

It can be seen that the magnetic field distributions of the 2d racetrack and the 2d rectangle, of the 3d racetrack and the 3d rectangle are quite similar, respectively, so here we only analyze the difference between the 2d racetrack and the 3d racetrack. The magnetic flux of the track is provided by the long side of front and back and the short side of the left and right. Field distribution on the XZ plane shows that all receivers have good coupling with the long sides of the track which is relatively narrow, while YZ distribution indicates that coupling situation between receiver and short sides varies with track length and receiver position. For the 2d racetrack, when the receiving coil is biased to the left, the central flux is mainly provided by the left area φ_{m1A} (red area) while the right area provides a small amount of flux φ_{m1B} (green area). When the receiving coil moves to the center, the central flux is provided by both sides, and the overall flux is relatively strong and stable. As for 3d racetrack, when the receiving coil is offset to the left, the flux is mainly supplied by the left area φ_{m1A} and right area distributes little due to long distance. When the receiving coil moves one-unit distance, the magnetic flux of φ_{m1A} decreases little, and there is little part flux from the right side. When the receiving coil moves to the center, the magnetic flux provided by left side and right side are both relatively weak. Therefore, there is fluctuation of coupling strength since the magnetic flux increases first and decreases when receiving coil moving from one side to the center of a 3d racetrack. To sum up, the 2d transmitting track has relatively more stable magnetic flux than that of 3d.

As shown in Figure 7, it is obvious that the racetrack has a slightly higher coupling coefficient than the rectangle track with the same length, and the short track shows better performance than the long track of the same shape. More detailly, for both 2d racetrack and 2d rectangle, the coupling coefficient is higher at middle of the track than that at two sides. For 3d racetrack, the coupling coefficient first increases and then decreases when receiving coil moves from side to the middle of the track, and the 3d rectangle track shares the same trend.
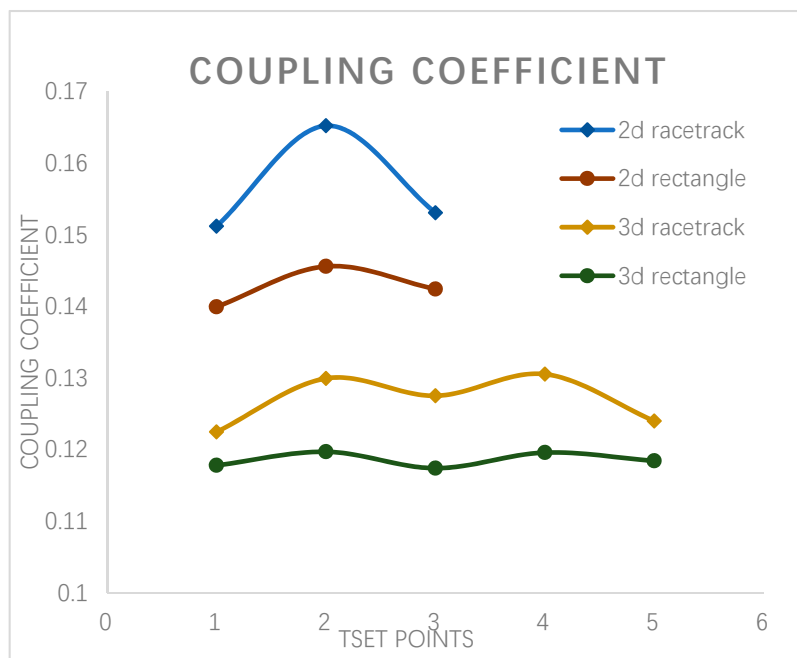
Figure 7. Coupling coefficient at different points.

3.2.2. Track Length Analysis with Multi Receiving Coils

All of the above analysis is for a single receiving coil. In order to explore the optimal length of long track while powering multiple coils, we are now set a series of models having 1, 2, 3 receiving coils respectively. For each model, a receiving coil occupies the same length of track, 2d, and magnetic field contribution is shown in Figure 8, while the coupling coefficient is listed in Table 4.
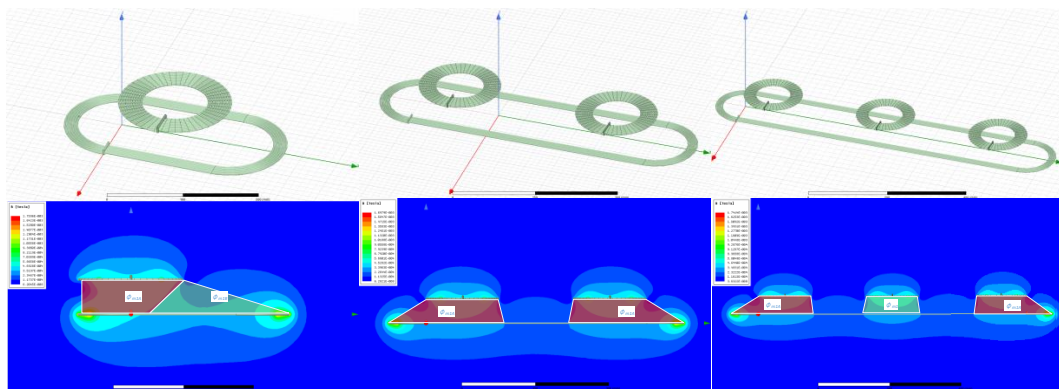

Figure 8. Models and magnetic field distribution of 2d, 4d, and 6d racetracks.

Table 4. Coupling coefficient of different receiving coil.

Parameter	4dracetrack	6dracetrack
Coupling coefficient between track and receiving coil 1/k_1	0.1092	0.09044
Coupling coefficient between track and receiving coil 2/k_2	0.1098	0.08574
Coupling coefficient between track and receiving coil 3/k_3	-	0.09044
Coupling coefficient between adjacent receiving coils	0.004620	0.003797
Sum of coupling coefficient of receiving coils	0.2190	0.26662

The magnetic distribution of the 2d, 4d and 6d racetrack configurations shown in Figure 8 clearly display that with the receiving coil in the left side, it has flux mainly supplied by the left side and partly by the right side for 2d racetrack, while the flux is only provided by the left side for 4d and

6d racetrack. When the receiver moves to the center, the flux supported by the left and right sides is weaker for increased track length from 2d to 3d, 6d. Therefore, the overall magnetic field strength is decreasing with the increase of track length.

Comparing the average coupling coefficient between the 2d racetrack, the 4d racetrack, and the 6d racetrack with single receiving coil respectively, it is clear that coupling coefficient decreases while the track length increases, but the rate of decreasing has slowed down. Take a look at the overall system, the added-up coupling coefficient is increasing with the track length under the condition that receiving coils are evenly distributed and the ratio between the length of the track and the number of receiving coils is the same. As shown in Tables 3 and 4, the sum of coupling coefficients of the 2d, 4d, and 6d racetracks are 0.1653, 0.2190, and 0.26662 respectively. Moreover, when the adjacent coils are separated by the length of their own diameter, the coupling between them is very weak, with 0.004620 of 4d racetrack and 0.003797 of the 6d racetrack, which can be ignored.

4. Experimental Verification

As shown in Figures 9 and 10, circular receiving coil and transmitting tracks of different shapes and lengths, exactly same with simulation parameters set in Table 2, with transmitting tracks wrapped 6 turns and receiving coil wrapped 10 turns with litz wire of 3 mm diameter to testify the feasibility and accuracy of the simulation and optimization algorithm. Same with simulation method, the output power and efficiency are tested with both transmitting track and receiving coil static from point to point. Besides, as presented in Table 5, the system is powered by a 10 V power supply, the track and receiving coil are separated by a 50 mm thick foam box, the system adopts SS topology with 100 kHz operating frequency and the load of the system is an adjustable resistor which is fixed at 10 Ω during the test.
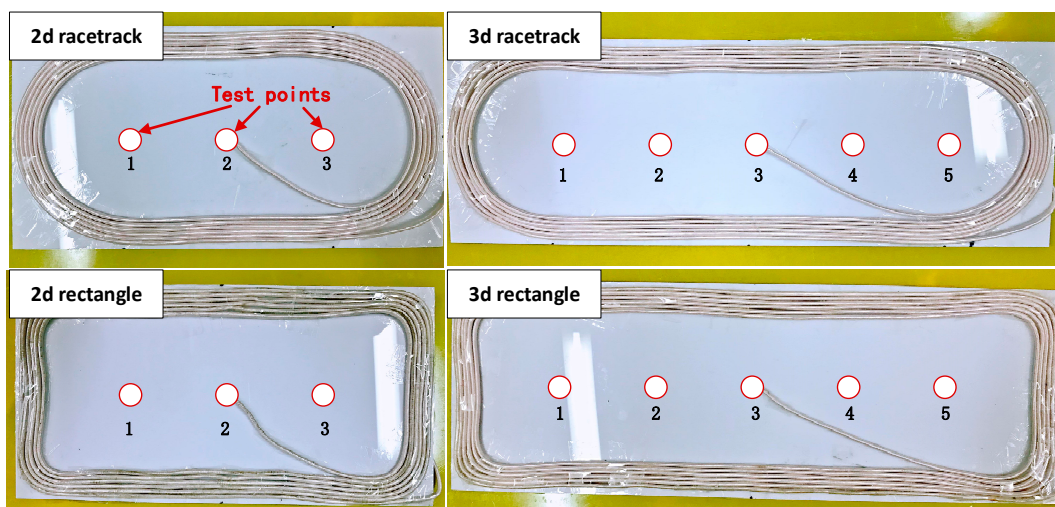

**Figure 9.** Transmitting track with different shape and length.

Figure 10. Receiving coil.

Table 5. Experiment related parameters.

Parameter	Value
Input voltage	10 V
Operating frequency	100 kHz
Inductance of receiving coil	17.5 μH
Inductance of 2d racetrack	17 μH
Inductance of 2d rectangle	19 μH
Inductance of 3d racetrack	24.3 μH
Inductance of 3d rectangle	26 μH
Resistance	10 Ω

The receiving circular coil, of 10 turns and 15 cm outer diameter are aligned with transmitting track at the test points from 1 to 3 or 5, where the voltage and current of both primary side and secondary side are measured with a 10Ω load respectively to calculate the system efficiency. And the test data is elaborated in Table 6 and intuitively shown in Figure 11.

Table 6. Test data for different tracks.

Parameter	Primary Voltage/V	Primary Current/A	Input Power/W	Secondary Voltage/V	Secondary Current/A	Output Power/W	System Efficiency/%
2d racetrack	10	4.02	40.2	16.11	1.53	24.6483	61.3142
	10	4.19	41.9	16.52	1.56	25.7712	61.5064
	10	4.41	44.1	16.46	1.64	26.9944	61.2118
3d racetrack	10	4.28	42.8	16.26	1.53	24.8778	58.1257
	10	4.26	42.6	16.25	1.58	25.675	60.27
	10	4.53	45.3	16.63	1.59	26.4417	58.3702
	10	4.54	45.4	16.67	1.61	26.8387	59.1161
	10	4.84	48.4	17.16	1.65	28.314	58.5
2d rectangle	10	6.3	63	18.83	2.04	38.4132	60.9733
	10	5.9	59	18.56	1.95	36.192	61.3424
	10	5.9	59	18.5	1.94	35.89	60.8305
3d rectangle	10	4.82	48.2	17.01	1.62	27.5562	57.1705
	10	4.69	46.9	16.92	1.62	27.4104	58.4443
	10	4.92	49.2	17.19	1.66	28.5354	57.9988
	10	4.63	46.3	16.875	1.62	27.3375	59.0443
	10	4.67	46.7	16.92	1.6	27.072	57.97
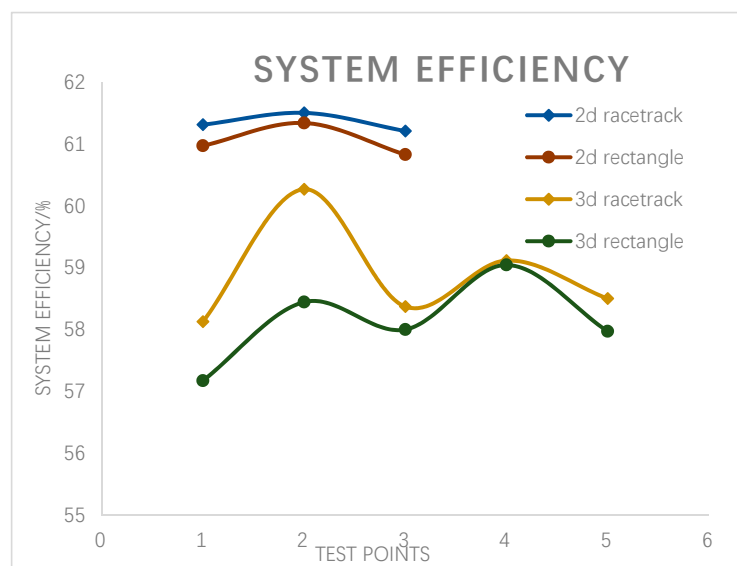
Figure 11. System efficiency of different tracks.

Looking at the system efficiency of 2d racetrack and 2d rectangle respectively, it can be observed that, for both, the efficiency is higher in the middle of the track than at the two sides. Moreover, the efficiency of the racetrack is higher than that of the rectangle track, which is consistent with the trend of coupling coefficient k in simulation results. By further analyzing the testing data of the 3d racetrack and 3d rectangle, it can be revealed that, for both tracks, the transmission efficiency first increases and then decreases when the receiving coil moves from the side to the middle of the track. Similarly, the efficiency of the 3d racetrack is better than that of the 3d rectangle track. To sum up, the racetrack has slightly better performance in terms of efficiency than rectangle track.

Comparing the system efficiency of the 2d racetrack with the 3d racetrack, and that of the 2d rectangle with the 3d rectangle, we can figure out that the overall transmission efficiency of the system decreases as the length of the transmitting track increases, showing good consistency with simulation results.

It is worth noting that the efficiency curves of the 3d racetrack and the 3d rectangle are not symmetrical, while theoretically they should be, to be consistent with the trend of coupling coefficient curve obtained by simulation. This may be caused by two errors. One is that the coil shape was not completely symmetrical due to manual winding error. The other is that there were some errors in the position of the receiving coil, which may have been inaccurate and resulted in the test points of the receiving coil being not precisely symmetrical

5. Conclusions

This paper first analyzes the advantages and disadvantages of a lumped power supply mode and a segmented rail power supply mode. Among them, the segmented rail power supply has higher reliability and stability, which is more achievable to apply. Then, four basic resonant compensation topologies were analyzed to find out that the SS resonance compensation topology is more feasible because the primary compensation capacitor is independent from load and mutual inductance, that is, the entire system can remain in the resonant state while load and coupling situation constantly change, which greatly reduces the control difficulty of the system. Based on the choice of rail mode and resonance compensation, this paper establishes the equivalent circuit and analyzes the output power and frequency characteristics of the system. Results show that when a single track is simultaneously coupled to multi receiving coils exceeding the upper limit, it will lead to the appearance of frequency bifurcation of SS-compensated system. Later, the circuit simulation is carried out and verified the correctness of theoretical analysis. Then the influence of the shape and length of the track on the coupling coefficient is analyzed. It is concluded that the performance of the racetrack coil is better than that of the rectangular track, and the coupling strength decreases with the increase of the track length. The experimental results are highly consistent with the results of the simulation analysis.

Author Contributions: Conceptualization, S.-C.Y. and H.H.; methodology, S.-C.Y.; software, H.H.; validation, H.H., X.-Y.Y. and Y.-H.C.; formal analysis, H.H.; investigation, Y.H.; resources, Y.-G.C.; data curation, J.L.; writing—original draft preparation, H.H.; writing—review and editing, Y.-G.C.; visualization, Y.H.; supervision, J.L.; project administration, H.-H.L.; funding acquisition, S.Y.

References

1. Li, S.; Liu, Z.; Zhao, H.; Zhu, L.; Shuai, C.; Chen, Z. Wireless Power Transfer by Electric Field Resonance and Its Application in Dynamic Charging. *IEEE Trans. Ind. Electron.* **2016**, *63*, 6602–6612. [CrossRef]
2. Budhia, M.; Boys, J.T.; Covic, G.A.; Huang, C. Development and evaluation of single sided flux couplers for contactless electric vehicle charging. In Proceedings of the Energy Conversion Congress and Exposition, Phoenix, AZ, USA, 17–22 September 2011.
3. Zhou, S.; Mi, C.C. Multi-Paralleled LCC Reactive Power Compensation Networks and Their Tuning Method for Electric Vehicle Dynamic Wireless Charging. *IEEE Trans. Ind. Electron.* **2016**, *63*, 6546–6556. [CrossRef]

4. Zhang, Z.; Pang, H.; Lee, C.H.T.; Xu, X.; Wei, X.; Wang, J. Comparative Analysis and Optimization of Dynamic Charging Coils for Roadway-Powered Electric Vehicles. *IEEE Trans. Magn.* **2017**, *53*. [CrossRef]

5. Buja, G.; Bertoluzzo, M.; Dashora, H.K. Lumped Track Layout Design for Dynamic Wireless Charging of Electric Vehicles. *IEEE Trans. Ind. Electron.* **2016**, *63*, 6631–6640. [CrossRef]

6. Zhang, Q.; Huang, Y.X.; Niu, T.; Xu, C. Analysis and Control of Dynamic Wireless Charging Output Power for Electric Vehicle. In Proceedings of the International Conference on Intelligent Computation Technology and Automation, Changsha, China, 9–10 September 2017.

7. Deng, Q.; Liu, J.; Czarkowski, D.; Bojarski, M.; Chen, J.; Hu, W.; Zhou, H. Edge Position Detection of On-line Charged Vehicles with Segmental Wireless Power Supply. *IEEE Trans. Veh. Technol.* **2017**, *66*, 3610–3621.

8. Tian, Y. *Research on Key Sectional Track-Based Wireless Power Supply Technology for Electric Vehicles*; Chongqing University: Chongqing, China, 2012.

9. Lu, F.; Zhang, H.; Hofmann, H.; Mi, C.C. A Dynamic Charging System with Reduced Output Power Pulsation for Electric Vehicles. *IEEE Trans. Ind. Electron.* **2016**, *63*, 6580–6590. [CrossRef]

10. Huh, J.; Lee, S.W.; Lee, W.Y.; Cho, G.H.; Rim, C.T. Narrow-width inductive power transfer system for online electric vehicles. *IEEE Trans. Power Electron.* **2011**, *26*, 3666–3679. [CrossRef]

11. Su, Y.C.; Jeong, S.Y.; Gu, B.W.; Lim, G.C.; Rim, C.T. Ultraslim S-type power supply rails for roadway-powered electric vehicles. *IEEE Trans. Power Electron.* **2015**, *30*, 6456–6468.

12. Park, C.; Lee, S.; Jeong, S.Y.; Cho, G.H. Uniform power I-type inductive power transfer system with DQ power supply rails for on-line electric vehicles. *IEEE Trans. Power Electron.* **2015**, *30*, 6446–6455. [CrossRef]

13. Mi, C.C.; Buja, G.; Su, Y.C.; Rim, C.T. Modern Advances in Wireless Power Transfer Systems for Roadway Powered Electric Vehicles. *IEEE Trans. Ind. Electron.* **2016**, *63*, 6533–6545. [CrossRef]

14. Choi, S.; Huh, J.; Lee, W.Y.; Lee, S.W.; Rim, C.T. New Cross-Segmented Power Supply Rails for Roadway-Powered Electric Vehicles. *IEEE Trans. Power Electron.* **2013**, *28*, 5832–5841. [CrossRef]

15. Yilmaz, T.; Hasan, N.; Zane, R.; Pantic, Z. Multi-Objective Optimization of Circular Magnetic Couplers for Wireless Power Transfer Applications. *IEEE Trans. Magn.* **2017**, *53*, 1–12. [CrossRef]

16. Zhang, W.; Wong, S.C.; Tse, C.K.; Chen, Q. An Optimized Track Length in Roadway Inductive Power Transfer Systems. *IEEE J. Emerg. Sel. Top. Power Electron.* **2014**, *2*, 598–608. [CrossRef]

17. Wang, C.S.; Covic, G.; Stielau, O.H. Power Transfer Capability and Bifurcation Phenomena of Loosely Coupled Inductive Power Transfer Systems. *IEEE Trans. Ind. Electron.* **2004**, *51*, 148–157. [CrossRef]

18. Villa, J.L.; Sallan, J.; Osorio, J.F.S.; Llombart, A. High-Misalignment Tolerant Compensation Topology for ICPT Systems. *IEEE Trans. Ind. Electron.* **2012**, *59*, 945–951. [CrossRef]

19. Okada, K.; Iimura, K.; Hoshi, N.; Haruna, J. Comparison of two kinds of compensation schemes on inductive power transfer systems for electric vehicle. In Proceedings of the Vehicle Power & Propulsion Conference, Seoul, Korea, 9–12 October 2012; pp. 766–771.

20. Bosshard, R.; Kolar, J.W.; Muhlethaler, J.; Stevanovic, I. Modeling and η-α-Pareto Optimization of Inductive Power Transfer Coils for Electric Vehicles. *IEEE J. Emerg. Sel. Top. Power Electron.* **2015**, *3*, 50–64. [CrossRef]